Proc. ESA Annual Meeting on Electrostatics 2010, Paper K4

Numerical Simulation of Trichel Pulses in a Negative Corona Discharge in Air

P. Sattari, G.S.P. Castle, and K. Adamiak
Dept. of Electrical and Computer Engineering
University of Western Ontario
phone: (1) 519-661-3030
e-mail: psattari@uwo.ca

***Abstract*—In this paper a new two-dimensional model is presented for the simulation of Trichel pulses in negative corona in a point-plane configuration. Both radial and axial components of the electric field are considered and it is assumed that three ionic species exist in the air gap: electrons, and positive and negative oxygen ions. The Poisson equation is solved for the electric field in the gap and three continuity equations are solved for modeling the transport of the charge species in the air gap. The Finite Element Method (FEM) is used for solving the Poisson equation and a combined Flux Corrected Transport-FEM is used for the charge transport equations. The algorithm is able to reproduce pulses and shows that with increased voltage the pulse frequency decreases in agreement with previously reported experimental data.**

I. INTRODUCTION

As the negative voltage applied to the point in the point-plane geometry in electronegative gases is increased, different phases of negative corona appear. Goldman and Goldman [1] have classified these phases to (1) auto-stabilization, (2) regular pulses and (3) continuous current discharge. Phase (2) is called the Trichel pulse regime after Trichel [2] and it occurs within a certain voltage range. In oxygen and air these pulses are very regular, but in some other gases, like SF_6, they are more irregular [3]. The Trichel pulses only occur in electronegative gases, i.e. those which have affinity for electrons. In electropositive (non-attaching) gases such as nitrogen, the corona current in the external circuit would be continuous without pulses.

Trichel pulses are normally very regular with very short rise times (as short as 1.3 ns [4]) and very short durations (tens of ns [5]) separated by longer inter-pulse periods (tens of μs [5]). Trichel reported the existence of such pulses in oxygen. It was observed that the frequency of the pulses varies linearly with the corona current and also was a function of the point diameter varying as an inverse function of the radius of the point for the same corona current. It was also observed that the frequency of the pulses is not a function of gap length, but varies with current independent of gap length. Trichel was able to explain some very important features of the corona discharge, like the shielding effect produced by the positive ion cloud near the cathode.

Loeb et al [6] confirmed that these regular pulses exist only in electronegative gases. He tried to explain this phenomenon by presenting a theory which involved successive electron avalanches, each giving rise to three successors near the end of its development. But this theory could not explain the fast rise time of 1.5ns observed in air at atmospheric pressure.

Lama and Gallo [7] carried out a series of carefully designed experiments to determine the dependence of pulse frequency, charge per pulse, and time averaged corona current on the applied voltage, needle tip radius, and needle to plane spacing. They also tried to explain the physical mechanism of the corona discharge.

Several scientists have tried to explain the periodic character of the discharge. Trichel [2] himself predicted that the space charge formation and subsequent clearing in the gap is the cause of the periodic character of the discharge. A negative cloud of space charge is formed far from the point and a positive cloud is formed near the point. The presence of positive ions near the point increases the field in this area and decreases the electric field between the positive ion cloud and the negative ion cloud. So, no ionization can take place beyond the positive ion cloud. The positive ions move towards the point under the effect of the electric field and narrow the region of enhanced electric field and finally the ionization process stops.

Aleksondrov [8] presented the theory of parallel development of several avalanches rather than successive avalanches. The faster rise times and the slowly rising current in the initial phase before the main pulse could be predicted by this theory. Kekez et al [9] used an equivalent circuit for the point-to-plane corona discharge and described the succession of pulses. However, his model could not explain the detailed mechanism of the pulse formation.

Ogasawara [10] presented an analytic solution which could describe the early stages of the rising current. However, his model could not predict the Trichel pulses as it just showed an exponential grow in the current. It was also unable to describe the role of negative ions in the discharge.

In 1985, Morrow [11], [12] proposed a one-dimensional model for the development of Trichel pulses by applying the combined Finite-Difference and Flux-Corrected Transport technique to solve the set of continuity equations along with Poisson's equation. He could only model the first Trichel pulse and offered a theoretical explanation for the different stages of the pulse. His work was the best-known among all the attempts for theoretically explaining the corona discharge phenomena. The results agreed well with the experimental data on the current-voltage dependency and also on the dynamics of the pulse initiation. However, the extension of the calculations to longer times showed only continuing decay of the current without subsequent pulses. Although he did explain the different stages of the pulse he ignored the ion secondary emission.

Napartovich et al [13] proposed a 1.5D numerical model for the analysis of Trichel pulses. They could model the sequence of Trichel pulses in dry air for short gaps (<1cm). Some other authors used simplified models in order to model chains of Trichel pulses [9], [14] and [15].

In this paper, a new two-dimensional numerical model incorporating three ionic species for the negative corona discharge in air is presented. A series of Trichel pulses for different applied voltages is successfully shown. In addition, the electron and ion densities dur-

ing the different stages of Trichel pulse are presented. The electric field is calculated by means of the Finite Element Method (FEM) and the hybrid FEM-Flux-Corrected Transport (FCT) technique is utilized for the space charge density calculations.

II. MATHEMATICAL MODEL

A. Governing Equations

Fig. 1 shows the configuration of the needle-plane system used for three species modeling of corona discharge. A hyperbolic needle with a tip radius curvature R and length L is mounted perpendicularly to an infinitely large plate at a distance d. Negative potential V_c is applied to the needle. An external resistance R_{ext} is connected in series with the needle - ground plate. The ambient gas is air at room temperature and atmospheric pressure.

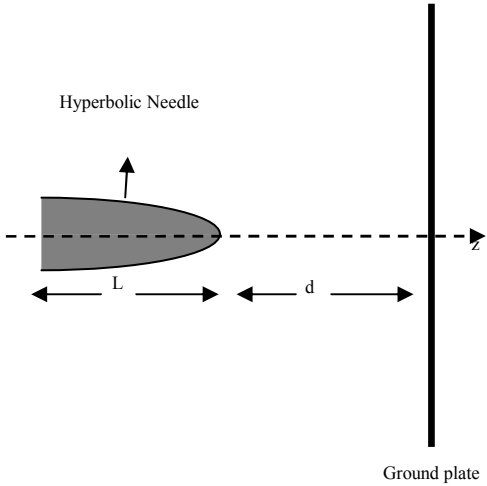

Fig.1. The configuration of corona discharge system.

The magnetic effects in the considered problem are negligible because of very low currents densities. Therefore, the electric field can be simulated using the following equations:

$$\nabla \cdot \vec{D} = (N_p - N_e - N_n) \tag{1}$$

$$\vec{D} = \varepsilon_0 \vec{E} \tag{2}$$

$$\vec{E} = -\nabla V \tag{3}$$

where $\vec{D}$ is the electrostatic displacement, $\vec{E}$ is the electric field, V is the electric potential, and ε_0 is the gas permittivity,

Equations (2) and (3) can be substituted in (1) to obtain Poisson's equation

$$\nabla^2 V = -\frac{(N_p - N_n - N_e)}{\varepsilon_0} \tag{4}$$

Electron density, positive ion and negative ion densities can be obtained by solving the following charge continuity equations:

$$\frac{\partial N_e}{\partial t} + \nabla \cdot (N_e \vec{W}_e - D_e \nabla N_e) = (k_i - k_a) N_e + k_d N_n - \beta_{ep} N_e N_p \tag{5}$$

$$\frac{\partial N_p}{\partial t} + \nabla \cdot (N_p \vec{W}_p) = k_i N_p - \beta_{ep} N_e N_p \tag{6}$$

$$\frac{\partial N_n}{\partial t} + \nabla \cdot (N_n \vec{W}_n) = k_a N_n - k_d N_n \tag{7}$$

In these equations: N_e, N_p and N_n are the densities of electron, positive ions and negative ions, respectively. $\vec{W}_e$, $\vec{W}_p$ and $\vec{W}_n$ are the drift velocities of electrons, positive ions and negative ions [16].

$$\vec{W}_e = \mu_e \vec{E}; \quad \mu_e = 0.05\, m^2/V \cdot s \tag{8}$$

$$\vec{W}_p = \mu_p \vec{E}; \quad \mu_p = 2 \times 10^{-4}\, m^2/V \cdot s \tag{9}$$

$$\vec{W}_n = \mu_n \vec{E}; \quad \mu_n = 2 \times 10^{-4}\, m^2/V \cdot s \tag{10}$$

k_i, k_a and k_d are the ionization, attachment and detachment coefficients and are equal to [16]:

$$k_i = 10^{11.93 - \frac{4.493}{EN}} \text{ (1/s)}, \; k_a = 6 \times 10^6 \text{ (1/s)}. \; k_d = 0$$

$EN = \dfrac{E \times 10^{21}}{NO_2}$; E is the magnitude of electric field in V/m and NO_2 is the number density of oxygen molecules which is approximately equal to 2.46×10^{25} ($1/m^3$) under standard pressure and at room temperature [17].

β_{ep} is the electron-positive ion recombination coefficient and is equal to [16]:

$$\beta_{ep} = 5 \times 10^{-13} \text{ } (m^3/s)$$

D_e is the diffusion coefficient of electrons and is equal to [17].

$$D = \frac{k_B T \cdot k}{e_0} \tag{11}$$

where k_B is the Boltzmann constant which is equal to 1.38065×10^{-23} $m^2kgs^{-2}K^{-1}$, T is the absolute temperature, e_0 is the electron charge, equal to 1.602×10^{-19} C.

B. Boundary Conditions

The corona electrode and ground are equipotential. Therefore, the boundary conditions for voltage are:

$V = V_c$-IR_{ext} on the corona electrode.

$V = 0$ on the ground plate.

The continuity equations for negative and positive ions are of first order. Therefore the boundary conditions for negative ions and positive ions are:

$N_p = 0$ on the ground plane

$N_n = 0$ on the corona electrode.

Since the charge continuity equation for electrons is a second order differential equation, it needs two boundary conditions. The first condition is that the normal derivative of electron is zero on the ground electrode. The value of electron density at different points of the corona electrode is the second required boundary condition and is obtained using the secondary electron emission:

$$N_{ec} = \gamma N_{pc} \frac{\mu_p}{\mu_e}$$

where γ is the secondary electron emission coefficient and is estimated to be equal to 0.01 [11].

III. NUMERICAL ALGORITHM

Since the electric field variations are very steep in both space and time, the solution algorithm should be chosen carefully. To capture the steep variations of electric field near the corona electrode, a non-uniform grid has to be used. This grid was made very fine near the corona electrode. In the remaining region, the electric field variation is more uniform; therefore, a coarser mesh was selected.

FEM was used for solving the Poisson equation. For the charge continuity equations, a combination of FEM and FCT proved to be a feasible technique. In this technique, artificial oscillations in the calculated results that occur when a classical FEM approach for the charge transport equations is used are removed using a three step procedure [19].

Initially, a small initial space charge density in the air gap was assumed, which represnts typical background ionization. Equations (4)-(7) were solved iteratively for one time step. The termination criterion of this iterative loop was that the change of the drift current in two successive iterations was less than δ_1 as given in (12). This condition was used to check the convergence of the corona electrode voltage, which changes due to the voltage drop on the external resistor. Also, this criterion was affected by the space charge convergence since if the space charge is convergent, the electric current, which is related to space charge will also be convergent.

$$\frac{I_{k+1} - I_k}{I_{k+1}} \le \delta_1 \qquad (12)$$

δ_1 was chosen arbitrarily, but was tested to give accurate results in a reasonable time period. Therefore, it was assumed to be 0.01 in our calculations.

When the electric field and space charge densities were found for one time step, the electron density on the corona electrode was updated from the secondary electron conditions. The same process was repeated for all the time steps.

Fig. 2 shows the flowchart of the simulation process and Fig. 3 illustrates the non-uniform FE grid used in the simulation. The mesh size close the corona electrode is in the order of 5μm.

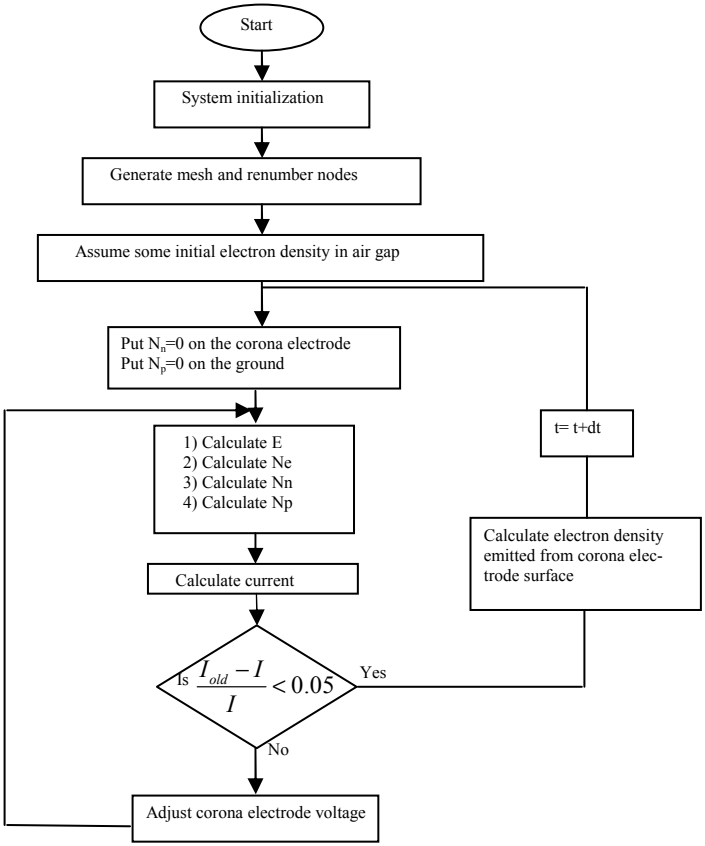

Fig. 2. Flowchart of the simulation algorithm

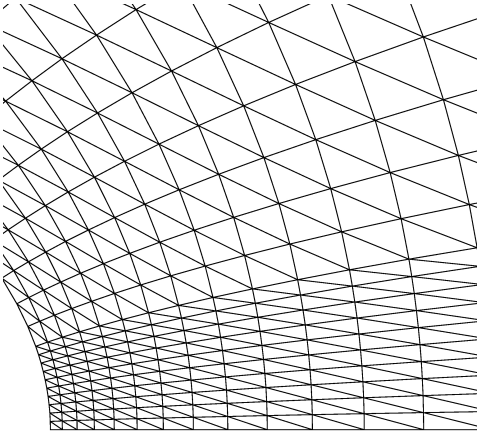

Fig.3. Details of FE grid near corona electrode used in the simulation process

IV. RESULTS

The hyperbolic needle is 1cm long (L=1cm) and is placed 1cm from the ground plate (d = 1cm). The radius of curvature R of the tip of the needle is 100μm. At the room temperature and atmospheric pressure the corona onset voltage for this configuration is evaluated to be 4.7 kV.

In this section the results of the numerical analysis showing a series of Trichel pulses for different applied voltages are presented. The behavior of the electric field and charge densities during one pulse is closely investigated. The distributions of charge densities along the axis of symmetry are compared at six different stages of one steady state pulse: i.e. at the beginning, half-pulse rising slope, maximum, half-pulse decreasing slope, after the pulse finishes, and after approximate steady state is reached . The electric field distributions along the axis are also presented. The numerical results showing the Trichel pulse period versus applied voltage for 7, 8, 9 and 11 kV are also compared with experimental data. Following are some detailed discussion of the 7 and 9 kV results.

A. Applied voltage = -7kV

A voltage of -7kV was applied to the needle-plane system and the corona current versus time is plotted in Fig. 4. Six sequential pulses are shown in this figure. The time distances between subsequent pulses are: 11.5μs, 13.38 μs, 10.67 μs, 10.85 μs and 10.4 μs. Therefore, after some initial variation the Trichel pulses become almost regular. The peak amplitudes of the pulses are approximately: 25mA, 2mA, 1.8mA, 1.8mA, 1.8mA and 1.8mA.

It was observed that the first pulse in the series of Trichel pulses always has a different behavior. Its amplitude is much larger than the rest of the pulses and the time interval between the first and second pulse is usually longer than the period of pulses in steady state. This difference in behavior can be explained by the fact that the first pulse is always produced in a charge-free space. There is no significant negative charge in the space to suppress the electric field in the ionization region. As a result, the maximum value of electric field for the first pulse is larger than its value for the rest of pulses. So, the ava-

lanche ionization is more intense and the total number of electrons and positive ions, which are created due to the avalanche ionization, is larger resulting in the larger corona current for the first pulse.

With regard to the time for the second pulse, the total number of negative ions created due to attachment during the first pulse is larger than the total number of negative ions created during the subsequent pulses. Therefore, these negative ions need more time to travel towards the ground. As a result, more time is needed for the electric field to increase above the value required for the appearance of the next Trichel pulse.

Fig. 6, 7 and 8 show the electron density, positive ion density and negative ion density along the axis of symmetry at different time instants for one typical Trichel pulse. These time instants are shown in Fig. 5.

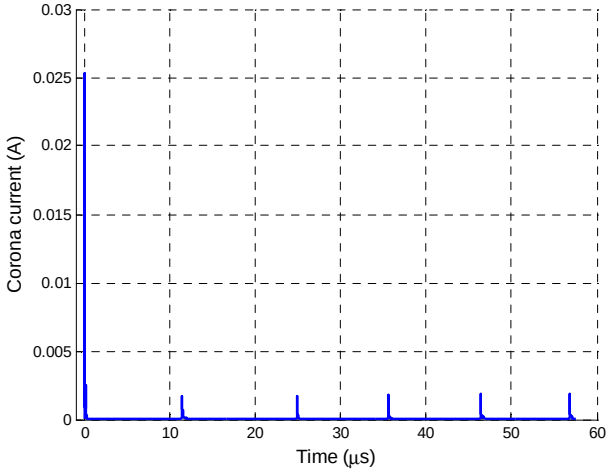

Fig.4. Trichel pulses for V= - 7kV

As Figure 5 shows, there is always a small post-pulse right after the main Trichel pulse. (the irregular local maximum right before instant 5 of Fig. 5). The explanation for the origin of this secondary pulse as follows. The first pulse is generated due to the avalanche ionization. This avalanche creates a large cloud of positive and negative charges. The decreasing of current right after the peak of the main pulse is due to the electric field reduction in the ionization layer caused by the existence of these clouds of ions. Later, movement of the positive ions towards the corona electrode creates a large amount of positive ions in the area close of the corona electrode and this increases the electric field in the very narrow ionization layer to the value required for another avalanche ionization. Therefore, the small pulse that will be generated after the first pulse is caused by the added ionization and movement of positive ions towards the corona electrode. These ions will soon be deposited on the electrode and they no longer create any further post-pulses. The second pulse can be a source of instability in the calculations. To avoid this, the time step needs to be chosen very carefully.

As Fig. 6 shows, electron density has very small values at the beginning of the pulse, then it starts increasing due to avalanche ionization and at the peak of the pulse (point 3), it reaches its maximum value. The electron density then starts decreasing and practically

disappears mainly due to the attachment to neutral oxygen molecules and also because of their rapid movement towards the ground due to the electric force.

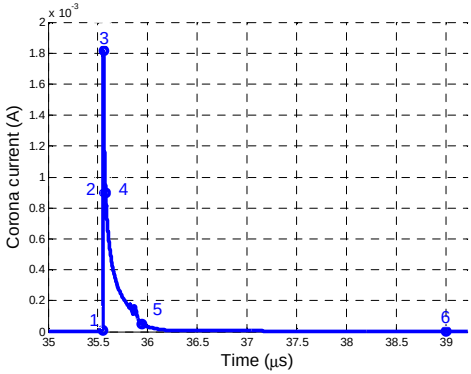

Fig. 5. Characteristic points on a typical Trichel pulse 1 - beginning of the pulse, 2 - half-pulse rising, 3 - maximum of the pulse, 4 - half-pulse decreasing, 5 - end of the pulse, 6 - 4 microseconds after the pulse

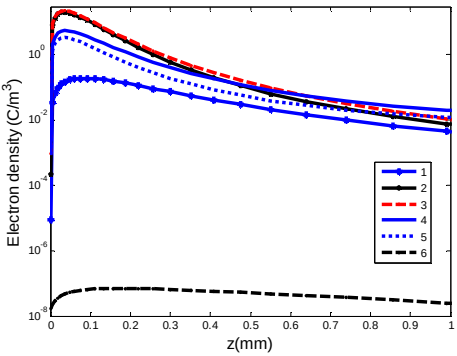

Fig. 6. Electron density along the axis of symmetry at different instants during a Trichel pulse

Fig. 7 shows the positive ion density along the axis of symmetry at different instants of time. The behavior of positive ions is very similar to that of electrons. There are very few positive ions at the beginning of the pulse, and then their number increases because of the avalanche ionization process. Similarly to electrons, at the peak of the current pulse, the density of positive ions reaches their maximum value.

As soon as the positive ions appear in the air gap, the electric field force attracts them towards the corona electrode and they start being deposited on the corona electrode. The mobility of positive ions is relatively small but since the distance they have to travel is also very small, they arrive to the corona electrode in a few nanoseconds. This deposition can be seen between point 2 and 3 on Fig. 7. As soon as the positive ions start depositing on the corona electrode, the electric field in the ionization layer decreases and, therefore, the thickness of the ionization layer is reduced. The reduction of the electric field and thickness of the ionization layer, limits the avalanche ionization process and it eventually stops when practically all positive ions are deposited on the corona electrode.

Fig. 8 shows the negative ion density along the axis of symmetry at different time instants. As this figure shows, the negative ion density increases with time due to attachment of electrons to neutral molecules, creating negative ions. The electric field pushes the negative ions towards the ground but their velocity is relatively small and the distance they have to travel is much longer than the distance the positive ions travel. This explains the reason for the very long time between Trichel pulses (in comparison with the Trichel pulse width). The existence of negative ions in the air gap decreases the electric field between the cloud and corona electrode. Therefore, it delays the time for the electric field to once again reach the threshold value required for avalanche ionization and the creation of a new Trichel pulse. As a result, before a new pulse can develop, the negative ions must move far away from the corona electrode.

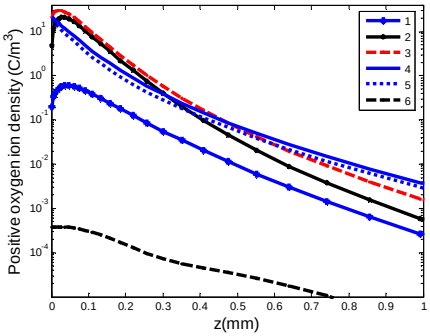

Fig. 7. Positive ion density along the axis of symmetry at different instants during a Trichel pulse

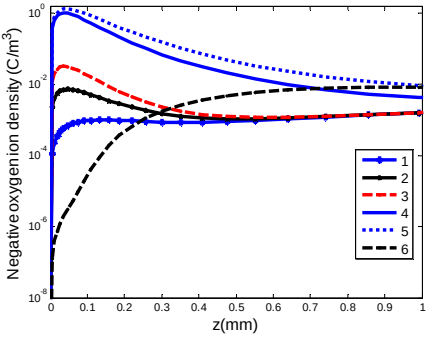

Fig. 8. Negative ion density along the axis of symmetry at different instants during a Trichel pulse

Fig. 9 shows the electric field intensity along the axis of symmetry at different time instants during a Trichel pulse. As this figure shows, at the beginning of the pulse, the electric field is large enough for the avalanche ionization to start. At point 2 which is the half pulse rising point, the positive ion and negative ion clouds are already created. The positive ion cloud, which is closer to the corona electrode, increases the electric field value in that area. Between the positive ion cloud and negative ion cloud the electric field decrease. This is shown in the curve 2 of this figure. At point 3, which is the maximum of the pulse, deposition has removed all the positive ions from the air gap and, therefore, the electric current starts decreasing after that point. By comparing curves 2 and 3, since the minimum of the electric field has not practically moved, it is clear that negative ions have not moved significantly and the distance of the point of maximum negative charge density from the corona electrode is about 0.025mm. At this point the electric field in the ionization layer has dropped below the threshold value and the main avalanche ionization has stopped. The negative ions then very slowly move towards the ground. At point 6, which is 4μs after the pulse, the negative ions have traveled considerably along the axis and electric field near the corona electrode has increased. These ions continue to move towards the ground electrode and the electric field at the corona electrode increases until the next pulse appears. This process repeats and the pulses are rather regular.

Fig. 10 shows the magnitude of electric field on the tip of the corona electrode versus time. The peaks in this figure represent the instants at which a Trichel pulse has appeared. Since the peak of the electric field depends on the amount of electrons and ions produced due to avalanche ionization, attachment and recombination, its value is different for each pulse. Between these peaks, the incremental change is relatively slow due to the very slow movements of negative ions.

As a further example of the information available from the two-dimensional model, Figures 11 and 12 show the densities of negative ions and positive ions in the air gap at the peak of the Trichel pulse. As these figures confirm, the electrons and positive ions form two clouds very close to the corona electrode and are negligible in the rest of the air gap.

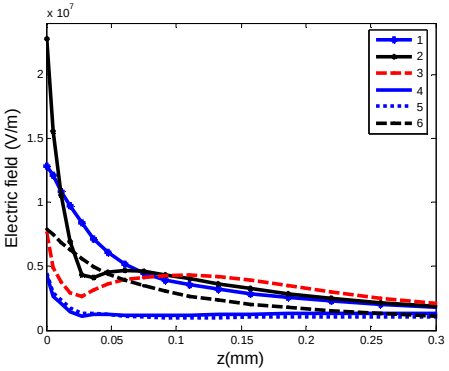

Fig. 9. Electric field along the axis of symmetry at different instants during a Trichel pulse

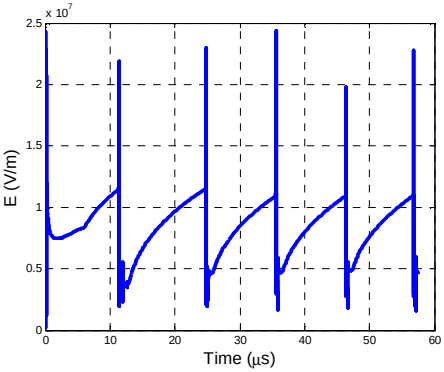

Fig. 10. Electric field versus time on the corona electrode

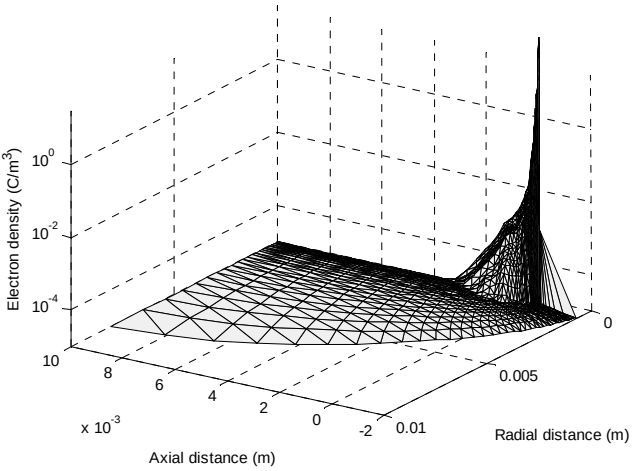

Fig. 11. Electron density in the air gap at the peak of the pulse

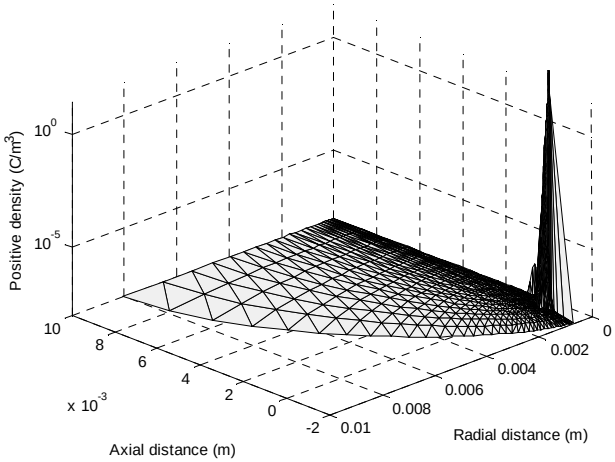

Fig. 12. Positive ion density in the air gap at the peak of the pulse

B. Applied voltage = -9kV

Fig. 13 shows the series of Trichel pulses for the applied voltage of -9kV. The amplitudes of subsequent pulses are approximately: 37mA, 1.68mA, 1.9mA, 2.03mA and 2.02mA. Distances between subsequent pulses are: 19.1 μs, 3.53 μs, 3.30 μs and 3.35 μs.

By comparing the period of the Trichel pulses for 7kV and 9kV, it can be seen that the frequency of these pulses increases with increasing the applied voltage. This agrees with the trend observed in previously reported experimental results [7].

Figures 14, 15 and 16 show the total number of electrons, negative ions and positive ions in the air gap as a function of time. As these figures show, the total number of electrons and positive ions between pulses is very small. Only during the Trichel pulse occurrence there is sudden generation of new charges. The negative ions are present in the air gap practically all the time, with a steady decrease between pulses and fast increase shortly after the pulse.

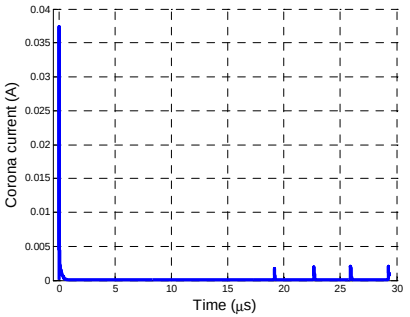

Fig. 13. Trichel pulse for V=-9kV

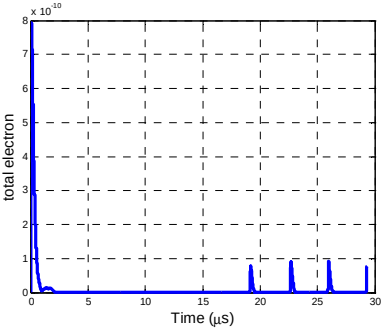

Fig. 14. Total electron charge in the air gap versus time

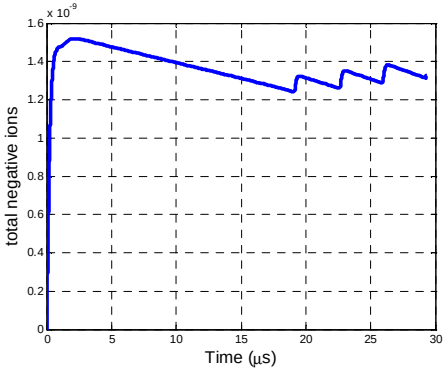

Fig.15. Total negative ion charge in the air gap versus time

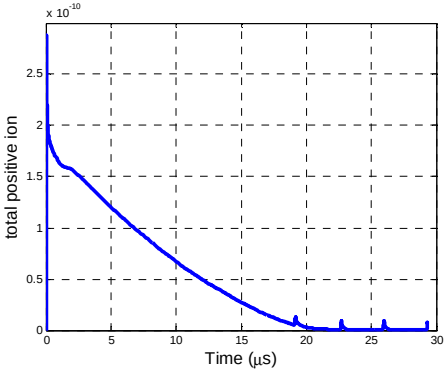

Fig. 16. Total positive ion charge in the air gap versus time

Fig. 17 and Table 1 show the Trichel pulse period for different applied voltages from the experimental data obtained by Lama and Gallo [7] alongside the average period of the numerical results obtained from our numerical technique. Fig 17 shows that the numerical data follow a similar trend line to the experimental results but tend to underestimate the periods by approximately 50%.

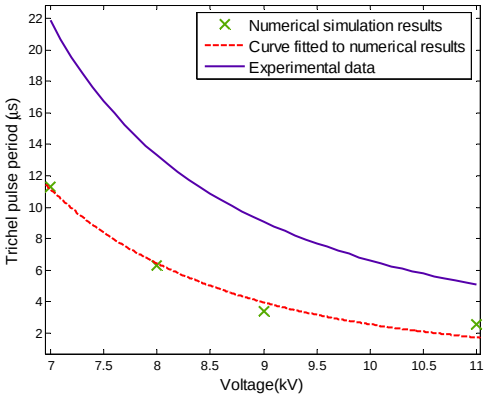

Fig.17. Trichel pulse period versus applied voltage: experimental data versus numerical results

TABLE 1: TRICHEL PULSE PERIOD VERSUS APPLIED VOLTAGE

Applied voltage	**7kV**	**8kV**	**9kV**	**11kV**
Numerical results for Trichel pulse period	11.33 μs	6.31 μs	3.39 μs	2.46 μs
Experimental data for Trichel pulse period	21.85 μs	13.32 μs	9.09 μs	5.07 μs

V. Conclusions

In this paper, a new two-dimensional FEM-FCT based model for three-species simulation of Trichel pulses in air is described. The model has successfully reproduced a series of Trichel pulses for different applied voltages and the pulse formation is explained by showing the densities of electrons, ions, and also the electric field distributions along the axis of symmetry.

To our knowledge, this is the first time the FEM-FCT based technique has been successfully applied for the 2D simulation of Trichel pulses for different applied voltages.

The results confirm that the frequency of the Trichel pulses increases as the applied voltage is increased. The numerical results obtained from this technique are compatible with previously reported experimental data available for Trichel pulse period versus voltage but underestimate the periods by approximately 50%. The reasons for this discrepancy are currently being further investigated and are believed to be related to some approximations within the numerical technique.

VI. Acknowledgement

The authors would like to acknowledge the helpful discussions and advices of C. F. Gallo during the course of this work.

References

[1] M. Goldman and A. Goldman, *Gaseous Electronics*, edited by M. Hirsh and H.J. Oskam, vol. 1, New York: Academic Press, 1978, pp. 219-290.

[2] G. W. Trichel, "The mechanism of the positive point-to-plane corona in air at atmospheric pressure," *Phys. Rev.*, vol. 55, pp. 382–390, 1938.

[3] R. J. Van Brunt and D. Leep,"Characterization of point-plane corona pulses in SF_6," *J. Appl. Phys.,* vol. 52, pp. 6588-6600, 1981.

[4] R. Zentner, "Ober die Anstiegzeiten der negativen korona entladung simpulse 2 angew," *Math. Phys.*, vol. 29, pp. 294-301, 1970.

[5] C. Soria, F. Pontiga and A. Castellanous, "Particle-in-cell simulation of Trichel pulses in pure oxygen", *J. Phys. D: Appl. Phys*., vol. 40, no. 15, pp. 4552-4560, August 2007.

[6] L. B. Loeb, A. F. Kip and G. G. Hudson, "Pulses in negative point-to-plane corona," *Phys. Rev.,* vol. 60, pp. 714–722, 1941.

[7] W. L. Lama and C. F. Gallo, "Systematic study of the electrical characteristics of the Trichel current pulses from negative needle-to-plane coronas," *J. Appl. Phys.*, vol. 45, pp. 103-113, 1974.

[8] G. N. Aleksondrov, "On the nature of current pulses of a negative corona," Sov. Phys. Tech. Phys., vol. 8, no. 2, pp. 161-166, 1963.

[9] M. M. Kekez, P Savic and G D Lougheed, "A novel treatment of Trichel-type phenomena with possible application to stepped-leader" *J. Phys. D: Appl. Phys.* vol. 15, pp. 1963-73, 1982.

[10] M. Ogasawara, "Analysis of formation stage of corona discharge," *J. Phys. Soc. Jpn*., vol. 21, no.11, pp. 2360-2372, 1966.

[11] R. Morrow, "Theory of negative corona in oxygen," *Phys. Rev.* A 32, pp. 1799–1809, 1985.

[12] R. Morrow. "Theory of stepped pulses in negative corona discharges," *Phys. Rev.* A 32, pp. 3821–3824, 1985.

[13] A.P. Napartovich, Y.S. Akishev, A.A. Deryugin, I.V. Kochetov, M.V. Pan'kin and N.I. Trushkin, "A numerical simulation of Trichel-pulse formation in a negative corona," *J. Phys. D: Appl. Phys.*, vol. 30, pp. 2726-2736, July 1997.

[14] J. M. K. MacAlpine and W C Yim, "Computer modeling of Trichel pulses in air," *Conf. on Electrical insulation and Dielectric Phenomena*, 1995, pp.118-21.

[15] P. A. Va'zqueza, A. T. Pe'rez, A. Castellanos and P. Atten, "Dynamic of electrohydrodynamic laminar plumes: scaling analysis and integral model," *Phys. Fluids*, vol. 12, no. 11, pp. 2809-2818, 2000.

[16] Yu, S. Akishev, M.E. Grushin, A.A. Deryugin, et al., "Formation of a two-dimensional model for Trichel pulse formation," TRINITI Report by Contract with the ABB Firm, 1997.

[17] J. Zhang and K. Adamiak, "A multi-species DC stationary model for negative corona discharge in oxygen: point-plane configuration," *J. of Electrostatics*, vol. 65, pp. 459-464, 2007.

[18] D. Kuzmin, and M. Möller, "Algebraic flux correction I. Scalar conservation laws," *In: Kuzmin, D., Löhner, R., Turek, S. (Eds.), Flux-Corrected Transport: Principles, Algorithms, and Applications,* New York: Springer, pp. 155-206.

[19] P. Sattari, G.S.P. Castle and K. Adamiak, "FEM-FCT Based Dynamic Simulation of Corona Discharge in Point-Plane Configuration," *IEEE Trans. on Ind. Appl.* (in press).